

Understanding brain connectivity from EEG data by identifying systems composed of interacting sources

Laura Marzetti^{a,b,*}, Cosimo Del Gratta^{a,b}, Guido Nolte^c

^a Department of Clinical Sciences and Bioimaging, Gabriele D'Annunzio University, Italy

^b Institute for Advanced Biomedical Technologies, Gabriele D'Annunzio University Foundation, Italy

^c Fraunhofer FIRST/IDA, Berlin, Germany

ARTICLE INFO

Article history:

Received 14 January 2008

Revised 18 April 2008

Accepted 24 April 2008

Available online 6 May 2008

Keywords:

Electroencephalography

Magnetoencephalography

Principal component analysis

Independent component analysis

Source interaction

Inverse methods

ABSTRACT

In understanding and modeling brain functioning by EEG/MEG, it is not only important to be able to identify active areas but also to understand interference among different areas. The EEG/MEG signals result from the superimposition of underlying brain source activities volume conducted through the head. The effects of volume conduction produce spurious interactions in the measured signals. It is fundamental to separate true source interactions from noise and to unmix the contribution of different systems composed by interacting sources in order to understand interference mechanisms.

As a prerequisite, we consider the problem of unmixing the contribution of uncorrelated sources to a measured field. This problem is equivalent to the problem of unmixing the contribution of different uncorrelated compound systems composed by interacting sources. To this end, we develop a principal component analysis-based method, namely, the source principal component analysis (sPCA), which exploits the underlying assumption of orthogonality for sources, estimated from linear inverse methods, for the extraction of essential features in signal space.

We then consider the problem of demixing the contribution of correlated sources that comprise each of the compound systems identified by using sPCA. While the sPCA orthogonality assumption is sufficient to separate uncorrelated systems, it cannot separate the individual components within each system. To address that problem, we introduce the Minimum Overlap Component Analysis (MOCA), employing a pure spatial criterion to unmix pairs of correlates (or coherent) sources. The proposed methods are tested in simulations and applied to EEG data from human μ and α rhythms.

© 2008 Elsevier Inc. All rights reserved.

Introduction

Non-invasive high temporal resolution functional imaging methods, such as electroencephalography (EEG) and magnetoencephalography (MEG), are well suited to study brain dynamics. Their millisecond temporal resolution can be exploited, in fact, not only to follow the variation of the activation patterns in the brain but also to track interference phenomena among brain areas. Recently, much attention has been paid to this second aspect (David et al., 2004; Horwitz, 2003; Lee et al., 2003), and many techniques aimed at studying brain connectivity have been developed and applied based on EEG potentials (Brovelli et al., 2002; Gevins, 1989) and MEG fields (Taniguchi et al., 2000; Gross et al., 2001). Frequency-domain methods are particularly

attractive in this sense since the activity of neural population is often best expressed in this domain (Astolfi et al., 2007; Gross et al., 2001; Pfurtscheller and Lopes da Silva, 1999). In the present work, a frequency domain approach is developed in which the imaginary part of the data cross-spectra at a frequency of interest is used to isolate true interference phenomena from the measured data. The imaginary part of the data cross-spectra is, in fact, the only part of complex cross-spectra that reflects true non-zero-lagged interactions in the brain. Hence, this quantity is insensitive to zero-lagged volume conduction effects (Nolte et al., 2004; Marzetti et al., 2007) that can be particularly problematic when describing interdependencies between signals (Gross et al., 2001; Nunez et al., 1997; Nunez et al., 1999). It can be shown that non-interacting sources do not contribute systematically to the imaginary parts of cross-spectra; therefore, this parameter is well suited to study brain interference phenomena (Nolte et al., 2004).

On the other hand, EEG and MEG measure a signal resulting from the superposition of the underlying brain source activities. In order to disentangle the contribution of the various brain

* Corresponding author. Institute for Advanced Biomedical Technologies (ITAB), Gabriele D'Annunzio University, Via dei Vestini, 31, 66013 Chieti, Italy. Fax: +39 08713556930.

E-mail addresses: laura.marzetti@gmail.com, lmazetti@unich.it (L. Marzetti).

sources to the measured signal, methods for the extraction of essential features based on linear transformations of the data space have been widely used. Among them, the well-known second-order methods such as principal component analysis (PCA) (Jolliffe, 1986) and factor analysis (FA) (Kendall, 1975) as well as methods based on higher order statistics such as independent component analysis (ICA) (Hyvarinen et al., 2001). We aim here at identifying the contribution of various sources and/or systems to the interaction phenomenon by decomposing the imaginary part of the cross-spectra. To this end, strategies for the identification of systems composed by interacting sources are developed in order to improve the understanding of the interaction phenomenon. We apply the proposed methods to simulated data and to real data from human μ and α rhythms.

Materials and methods

Problem formulation

We will first introduce some terminology used in this paper. By “source” we refer to functionally diverse neuronal units that are active in a specific rest or task condition. Each source has an activation time course and a specific spatial pattern in a sensor array (i.e., a specific orientation in the “sensor space,” in which each axis corresponds to the signal in one sensor). In this paper, we do not consider explicit time dependence as is possible, e.g., in event-related experiments. To study non-stationary effects, the necessary adjustments and re-interpretations are in principle straight forward but the details are beyond the scope of this paper.

It is assumed that the data were measured in a task-related experiment, i.e., processes are not explicitly time dependent. It is possible to generalize the concepts also to event-related experiments, but the necessary adjustments and re-interpretations are beyond the scope of this paper.

Let $\mathbf{x}(t)$ be the M -dimensional EEG/MEG data vector at time t . In this paper, we assume that these data can be decomposed as

$$\mathbf{x}(t) = \sum_{p=1}^P [\alpha_p(t)\mathbf{a}_p + \beta_p(t)\mathbf{b}_p] + \sum_{q=1}^Q \gamma_q(t)\mathbf{c}_q \quad (1)$$

where $\alpha_p(t)$, $\beta_p(t)$ and $\gamma_q(t)$ are the temporal activities of each source and \mathbf{a}_p , \mathbf{b}_p , and \mathbf{c}_q are the respective spatial patterns. $\gamma_q(t)\mathbf{c}_q$ are Q independent components, and $\alpha_p(t)\mathbf{a}_p$ and $\beta_p(t)\mathbf{b}_p$ are P pairwise interacting components, i.e., $\alpha_p(t)$ can be statistically dependent on $\beta_p(t)$ but neither on $\alpha_r(t)$ nor on $\beta_r(t)$ for $p \neq r$, and analogously for $\beta_p(t)$. We additionally assume that $P \leq M/2$ but we do not make restrictions on Q , the number of independent components. As a “compound system,” “interacting system,” or simply “system,” we refer to the activities denoted by a specific index p in the first sum in Eq. (1). A compound system hence consists of two temporal activities $\alpha_p(t)$ and $\beta_p(t)$, which are associated with two spatial patterns in channel space, \mathbf{a}_p and \mathbf{b}_p , respectively.

This model makes two assumptions. First, all interactions are assumed to be pairwise. For more complex interactions, the methods outlined below will approximate these systems by dominating pairs of interaction. Second, the number of compound systems measurable with EEG/MEG is assumed to be lower or equal than half the number of channels. Note that this assumption is considerably weaker than the typical assumption used for ICA, namely, that the total number of sources (which include, e.g., channel noise) is not larger than

the number of channels. Both assumptions are made for technical reasons. A generalization to arbitrary structure is welcome but is beyond the scope of this paper.

The goal of this paper is to identify the spatial patterns and to localize the sources of the interacting systems by analyzing cross-spectral matrices estimated from the data. Conceptually, this goal is achieved in three steps: (a) we analyze only imaginary parts of cross-spectra to get rid of systematic contributions from non-interacting sources; (b) we introduce a new method (sPCA) and recall an older one (PISA) both capable of identifying the 2D subspaces spanned by \mathbf{a}_p and \mathbf{b}_p for all p ; and (c) we introduce a new method (MOCA) to identify the patterns \mathbf{a}_p and \mathbf{b}_p themselves for a given 2D subspace. MOCA also includes the localization of the sources.

Principal component analysis and source principal component analysis (sPCA)

PCA is an orthogonal linear transformation that finds a representation of the data using only the information contained in the covariance matrix of the (zero mean) data vector. A new coordinate system for the data is chosen by PCA so that the largest variance by any projection of the data lies on the first axis (first principal component), the second largest variance on the second axis, and so on.

Again, let $\mathbf{x} = (x_1, \dots, x_m)^T$ be an M -dimensional EEG/MEG instantaneous data vector with mean value defined by $\mu_{\mathbf{x}} = E\{\mathbf{x}\}$. The notation $(\cdot)^T$ indicates matrix transpose.

Setting $\mathbf{x}_0 = \mathbf{x} - \mu_{\mathbf{x}}$, the zero-lag covariance matrix for that data set is defined as

$$\mathbf{C}_{\mathbf{x}} = E\{\mathbf{x}_0\mathbf{x}_0^T\} \quad (2)$$

Then, finding the principal components is equivalent to finding the eigenvalues and the eigenvectors of the covariance matrix by solving the eigenvalue equation:

$$\mathbf{C}_{\mathbf{x}}\mathbf{U} = \mathbf{U}\mathbf{\Gamma} \quad (3)$$

where $\mathbf{\Gamma}$ is a diagonal matrix of eigenvalues $\mathbf{\Gamma} = \text{diag}\{\lambda_1, \dots, \lambda_m\}$, and the columns of \mathbf{U} are the corresponding eigenvectors that form an orthogonal basis of the data space. For the calculation in the Fourier domain, the analogue of the covariance matrix is the cross-spectra matrix that is defined as

$$\mathbf{C}_{\mathbf{x}}(f) = E\{\hat{\mathbf{x}}_0(f)\hat{\mathbf{x}}_0^H(f)\} \quad (4)$$

where $\hat{\mathbf{x}}_0(f)$ is the Fourier transform of the Hanning-windowed demeaned data for each trial, $E\{\cdot\}$ is estimated by the average over these trials, and $(\cdot)^H$ denotes the Hermitian conjugate, i.e., transpose and complex conjugate.

When interpreting the eigenvectors of such matrices as potentials of single sources, two assumptions are made: (a) the sources are uncorrelated, and (b) the potentials are mutually orthogonal in signal space. Let's assume that the first assumption is correct and address the second one. The forward mapping of sources to sensors is essentially a spatial low pass filter. Even if the regions of non-vanishing source activities are spatially distinct, such as dipoles at different locations, which are orthogonal as vector fields, the respective potentials are highly blurred and are in general spatially correlated. Apparently, the orthogonality assumption would be much more reasonable if we were able to reconstruct the sources and formulate this assumption in source space.

The idea here is that, despite all limitations of inverse calculations, even rough estimates of the sources are spatially less correlated than the signals in channel space. For a practical implementation of this idea, we suggest to use a linear inverse method and then calculate the PCA decomposition of the cross-spectrum/covariance matrix in the source space (i.e., source PCA).

In general, results will depend both on the forward operator and the inverse operator. The most crucial question is whether sources, which are truly non-overlapping and hence orthogonal, give rise to non-orthogonal source estimates calculated from the respective scalp potentials. This will especially be the case if the true sources are close to each other and have similar direction. In this case, the decomposition will most likely be inaccurate. However, the key point here is that on average these inaccuracies are much lower than for PCA which will be shown in the simulations below.

A straightforward implementation if this idea faces a numerical problem: for K voxels and three dipole directions, the respective matrices have size $3K \times 3K$, which is in general too big to handle in a reasonable amount of time. Fortunately, for linear inverse methods, it is not necessary to make these calculations in such a large space, but, as will be shown below, it is also possible to formulate a non-symmetric eigenvalue problem in M dimensions that is formally equivalent.

Let A be an inverse operator of size $N \times M$, with $N = 3K$, considering three dipole orientations for each voxel, and $K \gg M$, mapping M measured signals to K brain sources (e.g., minimum norm operator). We can construct the source vector field estimated from the measurement vector \mathbf{x} as:

$$\hat{\mathbf{s}} = A\mathbf{x}. \quad (5)$$

The following is formulated for covariance matrices, but it is identical for cross-spectra. The covariance matrix for the sources, C_s , can be derived from the signal covariance matrix, C_x , as:

$$C_s = E\{\hat{\mathbf{s}} \cdot \hat{\mathbf{s}}^T\} = E\{(A\mathbf{x})(A\mathbf{x})^T\} = A E\{\mathbf{x}\mathbf{x}^T\} A^T = A C_x A^T \quad (6)$$

We now need to find the eigenvectors of C_s , i.e., we need to solve the Eq.

$$A C_x A^T \tilde{U} = \tilde{U} \tilde{\Lambda} \quad (7)$$

where $\tilde{\Lambda}$ is diagonal. In order to reduce the complexity of the eigenvalue problem in the source space, we multiply Eq. (7) from the left by $(A^T A)^{-1} A^T$ and insert the identity matrix $I = A^T A (A^T A)^{-1}$ after C_x , finally resulting in:

$$(C_x A^T A) (A^T A)^{-1} A^T \tilde{U} = (A^T A)^{-1} A^T \tilde{U} \tilde{\Lambda} \quad (8)$$

If we define a new matrix B as:

$$B = C_x A^T A \quad (9)$$

and

$$\hat{U} = (A^T A)^{-1} A^T \tilde{U} \quad (10)$$

then, from Eq. (7), it follows that:

$$B \hat{U} = \hat{U} \tilde{\Lambda}. \quad (11)$$

Thus, finding the eigenvectors of the huge Hermitian matrix C_s is reduced to finding eigenvectors of the small

non-Hermitian matrix B . Eigenvectors of B are in general not orthogonal. For non-vanishing eigenvalues, the eigenvectors \tilde{U} must be entirely in the space spanned by the sources, i.e., the range of A . Since $A(A^T A)^{-1} A^T$ is a projector on this space it follows that $A = A(A^T A)^{-1} A^T \tilde{U} = \tilde{U}$, i.e., the eigenvectors of the covariance matrix in source space (with non-vanishing eigenvalue) are given by the inverse mapping of the eigenvectors of the transformed covariance matrix in signal space.

In this way, the eigenvectors of B can be interpreted as the potentials/fields corresponding to temporally uncorrelated and spatially orthogonal sources in the brain. The respective sources can be estimated by applying the inverse operator A . It is also conceivable that the final source estimate is found by applying another inverse method on the decomposed fields—thus using the matrix A only as an intermediate tool to decompose the data. However, this specific interpretation is meaningful only for covariance matrices or real valued cross-spectra. Imaginary parts of cross-spectra require a different interpretation as outlined in the next section.

Decomposition of imaginary parts of cross-spectra

We are here interested in studying interaction by analyzing only imaginary parts (denoted C_I) of cross-spectra since these quantities are not biased by non-interacting sources regardless of the number of sources and regardless how the respective source activities are mapped into sensors (Nolte et al., 2004).

From a formal perspective, a straightforward way to do this is to decompose C_I into eigenvectors and then interpret these eigenvectors. However, the interpretation of these eigenvectors is not as straightforward as, e.g., for covariance matrices. Since C_I is real valued and antisymmetric, it is anti-Hermitian, and hence has only imaginary eigenvalues. Consequently, the eigenvectors can be neither purely real valued nor purely imaginary valued but must necessarily be a mixture.

Fourier transforming (Eq. (1)) and calculating the imaginary part the cross-spectrum leads to

$$\begin{aligned} C_I(f) &= \text{Im}(\langle \mathbf{x}(f) \mathbf{x}^H(f) \rangle) \\ &= \sum_p \text{Im}(\langle \alpha_p(f) \beta_p^*(f) \rangle a_p b_p^T + \langle \beta_p(f) \alpha_p^*(f) \rangle b_p a_p^T) \\ &= \sum_p \text{Im}(\langle \alpha_p(f) \beta_p^*(f) \rangle) (a_p b_p^T - b_p a_p^T) \end{aligned} \quad (12)$$

For simplicity of reading, we used the same symbol for functions in time and frequency domain.

If only one compound system consisting of two interacting sources with field patterns a and b are present, then C_I has the form

$$C_I \sim ab^T - ba^T \quad (13)$$

i.e., C_I is proportional to the antisymmetrized outer product of the two patterns. The important point now is that in general, apart from a global constant, C_I remains identical if we replace a and b by an arbitrary linear combination of a and b . It is therefore impossible to reconstruct from C_I the patterns a and b without additional knowledge. Note that assuming that the patterns are orthogonal is not sufficient to reconstruct these patterns. This reconstruction will be the subject of the next subsection, and we here continue with the decomposition into eigenvectors.

Without loss of generality, we now regard a and b as (unknown) linear combinations of the true patterns such that a

and \mathbf{b} are normalized and orthogonal to each other. Then \mathbf{C}_i has two eigenvectors with non-vanishing eigenvalues, namely, $\mathbf{a} + i\mathbf{b}$ and $\mathbf{a} - i\mathbf{b}$. Hence, the real and imaginary parts of these eigenvectors span a two dimensional subspace of the signal space identical to the space spanned by the fields of the sources or the estimates of the sources for PCA and sPCA, respectively.

If we have more than one compound system the eigendecomposition properly separates these systems provided that the orthogonality assumption is correct, i.e., $\mathbf{a}_p^T \mathbf{a}_r = \mathbf{a}_p^T \mathbf{b}_r$ for all $p \neq r$.

The above was formulated in channel space but applies identically in source space after replacing $\mathbf{x}(f)$, \mathbf{a}_p and \mathbf{b}_p with the respective sources estimated by using a linear inverse method. The only difference is that the orthogonality assumption, which was necessary for the interpretation of more than one compound system, has a different physical meaning.

We emphasize that sPCA is just standard PCA in source space and can be applied both to real and imaginary parts of cross-spectra (with different interpretation). Therefore, although we are here interested in brain interaction, we can test the different spatial assumptions of sPCA and PCA also for the simpler case of uncorrelated single sources which will be done below.

Pairwise interacting source analysis

The decomposition of the whole data into compound systems is also possible without making (spatial) orthogonality assumptions at all which can be achieved by the Pairwise Interacting Source Analysis (PISA) introduced by [Nolte et al. \(2006\)](#).¹ Here, instead of finding eigenvectors of $\mathbf{C}_i(f)$ at a given frequency f , one approximates $\mathbf{C}_i(f)$ simultaneously for all frequencies by a model

$$\mathbf{C}_i(f) \approx \sum_p \rho_p(f) (\mathbf{a}_p \mathbf{b}_p^T - \mathbf{b}_p \mathbf{a}_p^T) \quad (14)$$

with unknown $\rho_p(f)$, \mathbf{a}_p , and \mathbf{b}_p . The crucial model assumption is that the spatial patterns are independent of frequency. Apart from linear combinations of patterns *within* each compound system, this model can, in general, be identified uniquely if more than one frequency is considered. For technical details, we refer to the original publication ([Nolte et al., 2006](#)). The important point here is that PISA, like sPCA, is capable of identifying 2D subspaces spanned by the two patterns of each compound system, but is not capable of separating these 2D subspaces further into the patterns of the sources.

Minimum overlap component analysis (MOCA)

When studying interacting sources, the dynamical assumptions of sPCA only hold *between* different compound systems and therefore, it is meaningless to apply this method in order to disentangle the field patterns of the interacting sources *within* a compound system. Nevertheless, one can still use PCA or sPCA in order to get rid of noise and to reduce the dimensionality of the initial problem. As outlined above, if applied on imaginary parts of cross-spectra the resulting real and imaginary parts of the eigenvectors are then a linear combination of the fields of the two respective sources in the brain. When solving the inverse problem for these eigenvectors, in fact, a mixture of these

sources is localized. To the purpose of demixing these contributions MOCA was developed.

The MOCA approach solves the inverse problem for the real and imaginary parts of the eigenvectors found by PCA or sPCA. An inverse is already built in for the latter, but it is also conceivable to use standard PCA for the decomposition into systems and then proceed from there to decompose the eigenvectors into contributions from separate sources.

The inverse calculations of real and imaginary parts of an eigenvector give two source distributions $\mathbf{j}_1(\mathbf{x})$ and $\mathbf{j}_2(\mathbf{x})$, where, in practice, \mathbf{x} is a discrete variable denoting the respective voxel on a pre-defined grid within the brain. We assume that these two fields are superpositions of the true source-fields. (Here and in the following, the term “true source-field” used as an abbreviation for “correctly demixed estimates of the true source-fields.”) To find this superposition, we first assume, as in sPCA, that the true sources are spatially orthogonal. A transformation to orthogonal and normalized sources can be done with spatial pre-whitening. Let $\mathbf{\Sigma}$ be the 2×2 matrix with elements

$$\Sigma_{ij} = \sum_{\mathbf{x}} \mathbf{j}_i(\mathbf{x}) \cdot \mathbf{j}_j(\mathbf{x}) \quad (15)$$

Now we define $\mathbf{S} = \mathbf{\Sigma}^{-1/2}$ and define new sources as

$$\mathbf{k}_j(\mathbf{x}) = \sum_i S_{ji} \mathbf{j}_i(\mathbf{x}) \quad (16)$$

Note that this could also be written as a matrix multiplication by stacking voxel and dipole indices, but we consider the explicit formulation as clearer. Now, requiring orthogonal sources is not sufficient for a unique decomposition, as this property is conserved upon rotation:

$$\begin{pmatrix} \mathbf{m}_1(\mathbf{x}, \Phi) \\ \mathbf{m}_2(\mathbf{x}, \Phi) \end{pmatrix} = \begin{pmatrix} \cos\Phi & \sin\Phi \\ -\sin\Phi & \cos\Phi \end{pmatrix} \begin{pmatrix} \mathbf{k}_1(\mathbf{x}) \\ \mathbf{k}_2(\mathbf{x}) \end{pmatrix} \quad (17)$$

Now, the rotation angle Φ is fixed by assuming that the best source estimate is the one that minimizes the overlap between $\mathbf{M}_1(\mathbf{x}, \Phi)$ and $\mathbf{M}_2(\mathbf{x}, \Phi)$. For a meaningful definition of overlap, it should be defined to be invariant with respect to rotations of the coordinate system, and it also must be of higher order than (spatial) correlation in order to constitute an independent requirement. With these requirements, we consider as the most appropriate definition of overlap $L(\Phi)$:

$$L(\Phi) = \sum_{\mathbf{x}} (\mathbf{m}_1(\mathbf{x}, \Phi) \cdot \mathbf{m}_2(\mathbf{x}, \Phi))^2 \quad (18)$$

and we take as the final rotation angle Φ_{\min}

$$\Phi_{\min} = \arg \min (L(\Phi)) \quad (19)$$

Fortunately, minimization of $L(\Phi)$ can be done analytically in closed form. It is straightforward to check that the Eq. $L'(\Phi) = 0$ has the solutions

$$\Phi_0 = \frac{1}{4} \tan^{-1} \left(\frac{b}{a-c} \right) \quad (20)$$

with

$$\begin{aligned} a &= \sum_{\mathbf{x}} (\mathbf{k}_1 \cdot \mathbf{k}_2)^2 \\ b &= \sum_{\mathbf{x}} (\mathbf{k}_1 \cdot \mathbf{k}_2)(\mathbf{k}_1 \cdot \mathbf{k}_1 - \mathbf{k}_2 \cdot \mathbf{k}_2) \\ c &= \frac{1}{4} \sum_{\mathbf{x}} (\mathbf{k}_1 \cdot \mathbf{k}_1 - \mathbf{k}_2 \cdot \mathbf{k}_2)^2 \end{aligned}$$

¹ In that paper this method was termed ISA, which is now changed to avoid confusion with another method having the same name.

Various solutions arise due to the various branches of the \tan^{-1} function and differ by multiples of $\pi/4$. Minima and maxima are alternating, and we only have to calculate two neighboring solutions with angles Φ_{\max} and Φ_{\min} for the maximum and minimum, and pick the one referring to the minimum out of these two. We also note that

$$\text{gap} = \frac{L(\Phi_{\max}) - L(\Phi_{\min})}{L(\Phi_{\max}) + L(\Phi_{\min})} \quad (21)$$

might be used as a rough indicator of how well Φ_{\min} can be estimated. Specifically, if this *gap* is zero, then the cost-function has no unique minimum. This is, e.g., the case when the two sources are dipoles at the same location. The decomposition will result in two orthogonal dipoles but the orientation of the system as a whole is ill-defined.

Remark on weighted minimum norm inverse solutions

The methods presented here all require a linear inverse method, which are usually expressed as minimum norm estimates (Hämäläinen and Ilmoniemi, 1984, 1994; Wang et al., 1992). We here propose a specific variant of a weighted minimum norm solution that combines amplitude and geometrical properties of the forward model. The idea behind this is the consideration that minimum norm solutions typically are too superficial actually because of two different reasons. First and well known, superficial sources need smaller amplitude to induce a potential of given magnitude and are hence preferred. Second and perhaps less easy to understand is the fact that also the geometry biases the inverse solutions. The electric potential on the scalp is typically smoother for deeper sources. Qualitatively, to induce a potential of given (spatial) spectral content, superficial sources have to be more distributed to compensate for the weaker low-pass (a well-known consequence is that dipole fits of distributed sources typically are too deep; de Munck et al., 1988). Since the L_2 -norm becomes smaller if the source amplitude are distributed across several voxels, superficial sources are preferred.

In particular, we used a weighted minimum norm approach in which the source estimation is given by:

$$\hat{\mathbf{s}} = \mathbf{W}^{-1} \mathbf{L}^T (\mathbf{L} \mathbf{W}^{-1} \mathbf{L}^T)^{-1} \mathbf{x} \quad (22)$$

where \mathbf{L} is the leadfield matrix of size $M \times K$ provided by the EEG forward problem with $K = 3N$ for the N voxels of the grid, and \mathbf{W} is a diagonal weighting matrix of size $K \times K$. The elements of \mathbf{W} are defined to be independent of dipole direction as:

$$\mathbf{W}_{ii} = \frac{\|\mathbf{L}_i\|^q}{d_i^p} \quad (23)$$

where \mathbf{L}_i is the $M \times 3$ matrix where the j th column ($j=1\dots 3$) corresponds to the potential of a unit dipole at the i th voxel pointing in j th direction, the symbol $\|\cdot\|$ indicates the Frobenius norm, and d_i is the Euclidean distance between the i th voxel and the closest electrode. Eq. (20) with the settings $p=0$ and $q=1$ is the classical weighted minimum norm (WMNE) (Hämäläinen, 1993); see also Pascal-Marqui (1999) and Baillet et al. (2001) for comprehensive reviews. As outlined above, the classical WMNE has the problem that it estimates the location of a 3D current distribution closer to the electrode

or detector coil than its actual location (Crowley et al., 1989; Sekihara and Scholz, 1996; Pascal-Marqui, 1999). In order to overcome this limitation, we make a different choice for the parameter setting, in particular setting $p=1.5$ and $q=1$. With this setting, we add a factor penalizing the sources closer to the electrode that compensates for WMNE tendency to prefer such kind of sources. The exponent $q=1$ accounts for the amplitude and the exponent $p=1.5$ can be qualitatively understood as follows: in order to induce a potential with given (spatial) spectral content by a source located around depth d , this source has size $\sim d^{-1}$ and hence volume and number of active voxels are $\sim d^{-3}$. The reduction in the cost function from distributing the source activity across several voxels is proportional to the square root of the number of voxels, which is compensated in the cost-function. This rather heuristic argument could be confirmed in simulations of random single dipoles comparing the maximum of the estimated distributed source with the dipole location. We found a minimum deviation at $p=1.4$ in good agreement with the above considerations. We still take $p=1.5$ because we consider the argument, even if heuristic, as more generic than the specific simulation.

For MOCA, we regard its inverse solution part as a mere intermediate step to decompose a two-dimensional subspace of the signal space into two patterns. This intermediate step is done with weighted minimum norm solution using $q=1$ and $p=0$. The final inverse method for the decomposed field is chosen to be a depth-weighted minimum norm solution with $q=1$ and $p=1.5$. The reason for this difference is that the choice $q=1$ and $p=1.5$ has smaller bias to superficial sources for the price of having more widespread sources, and in simulations we found the choice $q=1$ and $p=0$ to be (slightly) better for the decomposition.

We want to emphasize that in the context of this paper the specific form of weights is a marginal issue. The proposed form appeared convincing to us, but we do not claim that our method is the best possible. Especially, we found the results to be similar to those from LORETA (Pascal-Marqui et al., 1999). A detailed comparison, however, is beyond the scope of this paper.

Simulations

The EEG montage consisted of 118 electrodes fitted to the outermost shell of a standard Montreal Neurological Institute (MNI) head (Evans et al., 1994), which was used as a three compartment realistic volume conductor model for the solution of the EEG forward problem (Nolte and Dassios, 2005). An electrode near the nasion was taken as reference. The source space was restricted to the segmented cortical surface of the MNI head based on the observation that primary sources are widely believed to be restricted to the cortex (Baillet et al., 2001). The sources were modeled as multiple current dipoles, apart from one case explicitly noted. The locations of the dipoles were randomly selected from the nodes of the triangularly tessellated cortical mantle, and the orientation was set normally to the cortical surface based on the physical orientation of the apical dendrites that produce the actual measured fields of the brain (Baillet et al., 2001).

In the following simulations, we test the appropriateness of the spatial assumptions made in sPCA and MOCA. This by itself is not restricted to the analysis of interacting sources. Specifically, sPCA is compared to PCA assuming uncorrelated sources

and hence assuming that the dynamical assumptions of PCA and sPCA are correct. In contrast, MOCA does not make dynamical assumptions, and we will test it both for correlated and uncorrelated sources and compare it to the respective results of PCA and sPCA. Note that the case of many pairs of correlated sources corresponds to the study of eigenvectors of imaginary parts of cross-spectra in the sense that the field patterns are a superposition of the true source patterns, which is completely unknown, whereas this superposition is partly known in the case of correlated sources. In other words, the spatial orthogonality assumption is sufficient for a unique decomposition of uncorrelated sources but not for correlated sources.

We will now give a general formulation for the configurations tested by our simulations. Given that N_0 is the number of ECDs in the simulation and M the number of channels in the EEG montage, the leadfield matrix L_0 of size $M \times N_0$ was derived for the ECD configuration, the montage and volume conductor described above by solving the EEG forward problem. We introduce for later use the source cross-spectrum matrix C_s of size $N_0 \times N_0$ and the noise covariance matrix C_n of size $M \times M$. The general model for the signal space cross-spectrum matrix, C_x of size $M \times M$, from which all the situations tested by our simulations can be derived, is:

$$C_x = L_0 C_s L_0^T + \alpha C_n \quad (24)$$

where α is a weight to the noise term such that the Frobenius norm of the source contribution to the signal cross-spectra is equal to the Frobenius norm of the noise term C_n . In the various simulations, we assume either that the dipole amplitudes are uncorrelated or are correlated with a positive definite covariance matrix. For the latter, we chose a different, randomly selected, source covariance matrix for each source configuration. Defining I_{N_0} as the identity matrix of size $N_0 \times N_0$ and S a matrix of Gaussian distributed random numbers of size $N_0 \times N_0$, the two cases are obtained by setting C_s respectively as:

$$C_s = I_{N_0} \quad (25)$$

$$C_s = S^T S. \quad (26)$$

We also assume various possible noise models by different settings of the C_n matrix. In particular, spatially correlated noise in the signal space (or equivalently uncorrelated noise in the source space) is described by setting:

$$C_n = LL^T. \quad (27)$$

Here is the leadfield matrix of all dipoles on the entire grid within the brain. Alternatively, a realistic noise is introduced in the simulations by setting C_n equal to a broadband mean value between 5 and 25 Hz of the real part of a cross-spectral matrix of actual EEG data C_m

$$C_n = C_m. \quad (28)$$

The last noise model describes the internal noise in the electronics of the measurement equipment and is spatially uncorrelated in the signal space. Defining as I_M the identity matrix of size $M \times M$, this noise model is obtained by setting:

$$C_n = I_M. \quad (29)$$

The above-defined different settings were used in order to analyze the performances of the proposed methods. In parti-

cular, in order to perform a systematic comparison between the PCA and sPCA methods for uncorrelated sources, 5000 pairs, triplets or quartets of uncorrelated dipoles were randomly placed on the cortex and the noise-free case as well as the three types of noise described above in Eqs. (22)–(24) were considered.

A second Monte Carlo simulation was carried out to investigate the accomplishment of the recovering of the true fields by PCA, sPCA, and MOCA for two uncorrelated or correlated ECDs with cross-spectra described in Eqs. (25) and (26), respectively. No noise was added in this case.

The performances of the methods in these simulations were evaluated by defining a global error accounting for the difference between the known field patterns and the recovered field patterns according to the equation

$$ERR = \sum_{i=1}^N \left(1 - \frac{|\tilde{v}_i^T \cdot v_{\Pi(i)}|}{\|\tilde{v}_i\| \cdot \|\tilde{v}_{\Pi(i)}\|} \right) = \sum_{i=1}^N (1 - |\cos \theta_{i\Pi(i)}|) \quad (30)$$

where \tilde{v}_i with $i=1, \dots, N_0$ are the true fields of each ECD; $v_{\Pi(i)}$ are the vectors (selected by a permutation Π) provided by the decomposition method, the symbol T denotes matrix transpose as above, and the symbol $\|\cdot\|$ indicates the Frobenius norm. The permutation Π , which has to be introduced because correspondence between eigenvectors and dipole fields cannot be predicted, was chosen by a greedy search: we first select a pair of closest patterns from the sets of true and estimated patterns, then take these two patterns out, find the pair of closest patterns from the remaining patterns, etc., until all true patterns are associated with an estimated pattern. The error can also be expressed in terms of the angle θ_{ij} between two patterns \tilde{v}_i and $v_{\Pi(i)}$ as given in the last term of (30) showing that the error vanishes if all respective pairs of patterns are proportional to each other.

Finally, for demonstration purposes, a simulation based on a pair of correlated extended and distributed source models is performed in order to test the performances of the proposed MOCA-WMNE method (Eqs. (21)–(22)) in comparison to the multiple ECDs localization in recovering this kind of source. A direct search for the location and orientation of multiple dipolar sources involves solving a highly non-convex optimization problem, which is prone to local minima. In order to avoid this potential problem, we use for the multiple dipole localization the signal subspace method, RAP-MUSIC (Mosher and Leahy, 1999), which is based on recursively removing the components of the signal subspace that are spanned by the explained sources. The source localization is performed in this simulation from the true simulated fields in order to show the plain effect of the source model in the localization results. The property of the two methods does not change if one provides the correctly disentangled field patterns as the input fields to the two inverse methods.

Actual EEG data

EEG data were collected from a 118-channel EEG cap during imagined left or right foot movement from (Blankertz et al., 2003). For each of the randomly mixed conditions, 70 imaginations, each lasting for ~3.5 s, were performed. Cross-spectra were calculated separately for each condition by linear detrending and Hanning windowing the 3.5-s windows and averaging over the respective 70 trials. To improve the signal-to-noise ratio, we additionally averaged the cross-spectra across

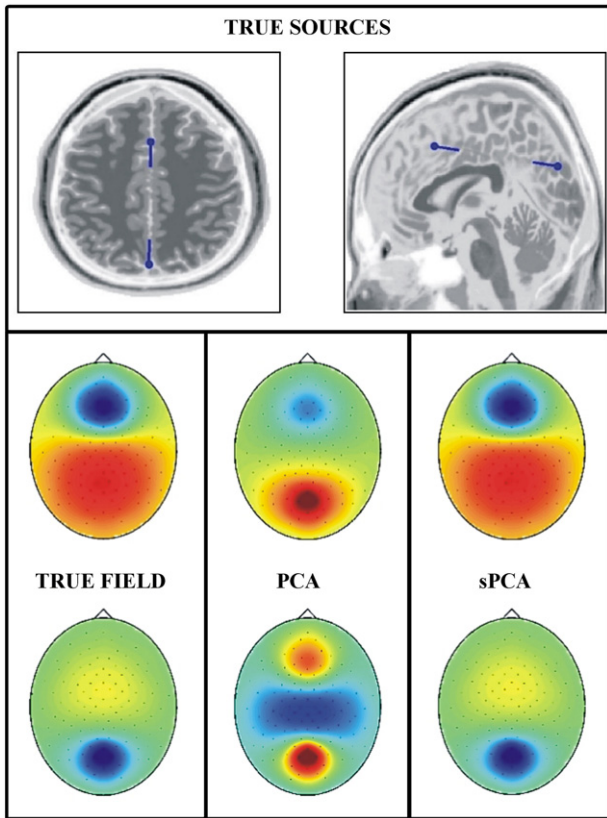


Fig. 1. Axial and sagittal views of the simulated source configuration are shown on the top. On the bottom, the true field patterns are compared to the PCA basis fields and to the sPCA basis fields.

neighboring frequencies with a Hanning window of width 11, leading to an effective frequency resolution of ~ 1 Hz. Since we are interested in studying interaction phenomena in the brain, we isolated from the whole complex cross-spectrum matrix the only part of it that necessarily reflects interactions, i.e., the imaginary part of the cross-spectra (Nolte et al., 2004).

Results and discussion

Simulations

Fig. 1 provides an example of classical PCA and of sPCA decomposition of the simulated field patterns generated by two uncorrelated ECDs (regarded here as the simplest configuration of a system). The true dipole fields are shown and compared to the result of the PCA decomposition and to the results of the sPCA decomposition. Clearly, PCA is not able to separate the field patterns of the two ECDs. The PCA eigenvectors, in fact, result in a combination of the true fields of both ECDs. Conversely, if the orthogonal assumption in the source space is exploited by applying sPCA to the field patterns a clear identification of the distinct dipole fields is possible.

Fig. 2 shows the results of this simulation for two dipoles, three dipoles and four dipoles. Each row in this figure is accounting for a different type of noise in the general model described in Eq. (21). On the x-axis of each subplot, the error between the true fields and the recovered ones as defined in Eq. (27) is reported, the corresponding occurrence of each error value over the 5000 runs is reported on the y-axis.

When no noise is added to the simulated data, sPCA outperforms PCA in recovering the true field patterns also for

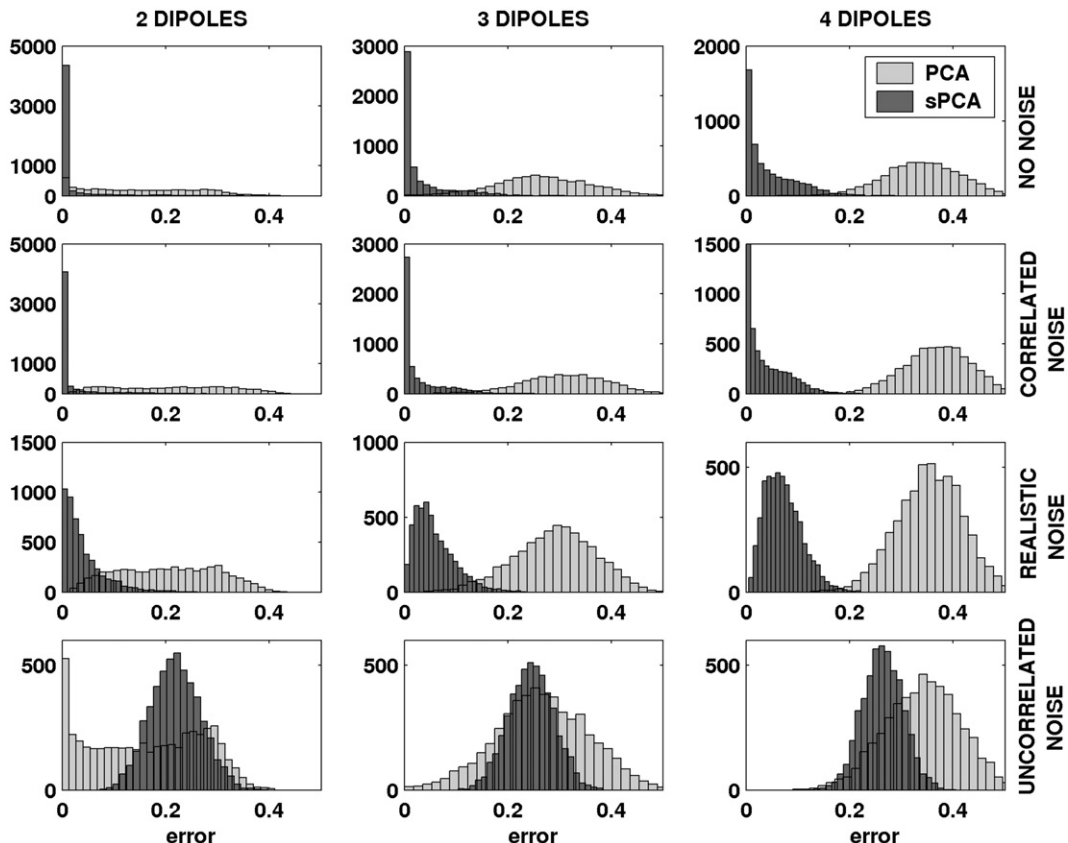


Fig. 2. PCA and sPCA error distributions for 2, 3, and 4 ECDs are shown. In each row a different noise is added to the simulated data.

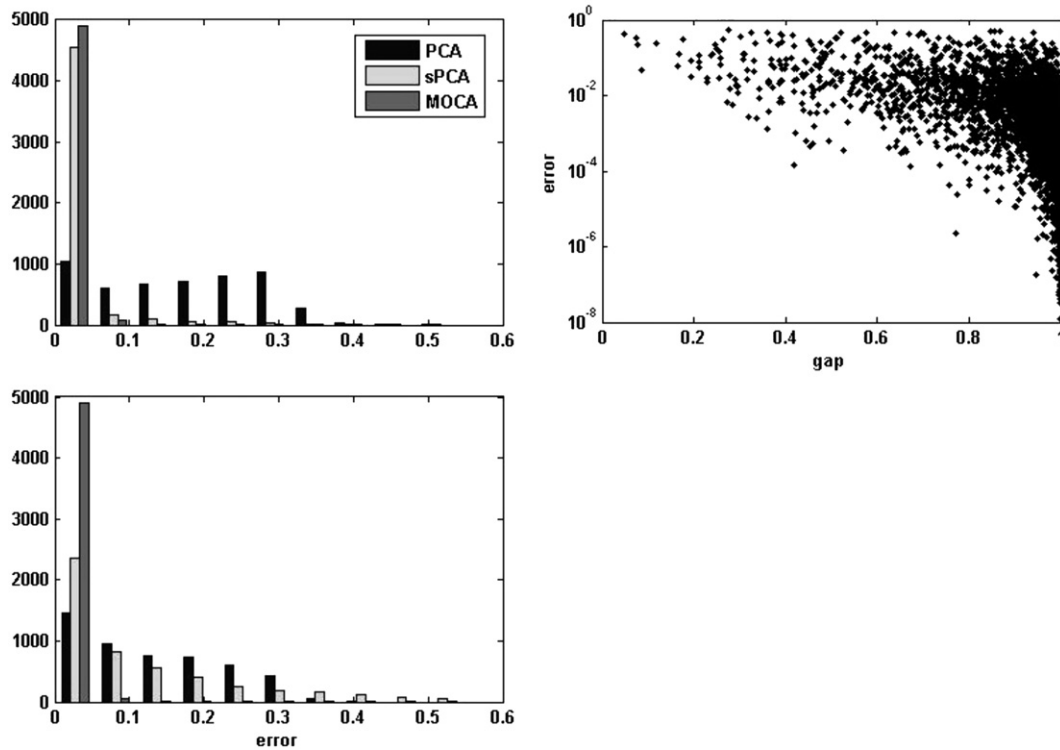


Fig. 3. The error distributions for PCA, sPCA, and MOCA are shown case of two uncorrelated and correlated ECDs. The scatter plot shows the relationship between the error of the MOCA method and the gap between the minimum and maximum of the MOCA cost function.

a higher number of dipoles. The error distributions for sPCA are centered on a median value that is at least 15 times smaller than the corresponding median value for the PCA error distribution. Furthermore, the PCA error distributions are typically wider than the corresponding sPCA, indicating a much higher occurrence of low error values for sPCA rather than for classical PCA. Note that some tails of the PCA distributions are cut in the plots.

Similar results were obtained also when uncorrelated noise in the source space was added to the data. This kind of noise is equivalent to the presence of spatially correlated noise in the

signal space, which is typically the case of spontaneous brain activity non-related to the neural activity under study (Sekihara and Scholz, 1996). In this case, the sPCA model is able to account for the uncorrelated noise in source space, which is correctly disentangled from the true fields. Conversely, classical PCA slightly degrades its performances with respect to the noise-free case.

When the noise model is constituted by realistic noise, the sPCA model is still able to explain such noise in terms of a field pattern orthogonal to the true fields, thereby succeeding in recovering the original field patterns. PCA performances are

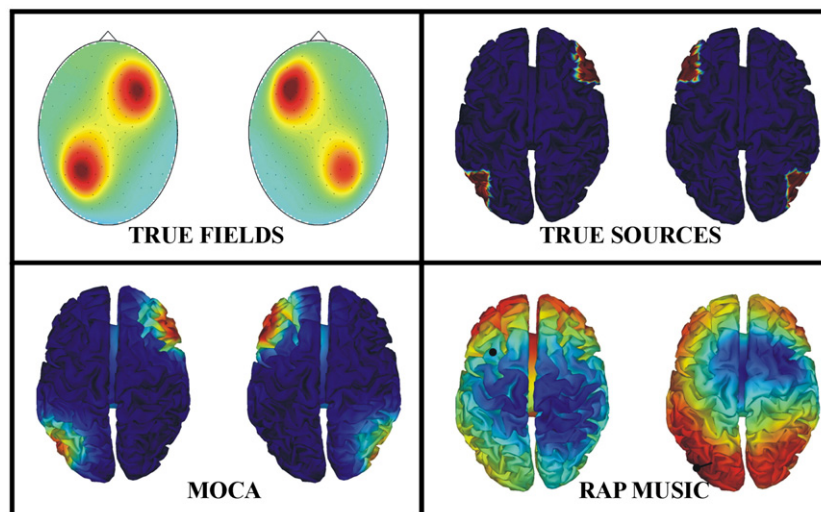


Fig. 4. The true field patterns generated from the true sources are given in input to MOCA-WMNE and to RAP-MUSIC. The sources are correctly recovered by MOCA-WMNE and wrongly recovered by RAP-MUSIC.

similar to the two previous cases. Since this kind of noise represents a realistic example of brain activity not related to the investigated neural activity in real EEG/MEG measurements, the success of sPCA in recovering the true fields is particularly valuable in this case.

In the presence of uncorrelated noise among all channels, we do not observe any advantage of sPCA over PCA. This is due to the fact that brain sources can hardly explain uncorrelated channel noise. In principle, it is possible to consider regularized inverse operators. However, uncorrelated channel noise is an unrealistic event that would mean that internal noise in the electronics of the measurement equipment is dominating the signal. Nevertheless, in this limiting case, sPCA performances become comparable to the PCA performances.

Fig. 3 shows the results for the second simulation in which the performances were evaluated also for a pair of correlated sources. The correlated structure of the sources is defined by a symmetric and in general non-diagonal source cross-spectrum as in Eq. (26). In this figure, a comparison of the MOCA results to PCA and sPCA results is shown in both cases of two uncorrelated or correlated sources. We want to underline here that the case of two correlated sources can be regarded as the separation of two correlated simple systems (each composed by one ECD) or equivalently as the separation of two correlated sources within a compound system. For the sake of simplicity, noise-free simulations have been performed in this case. The presence of noise can in fact be handled by the sPCA decomposition, as shown in Fig. 2, which can be applied as a prior step to MOCA.

For uncorrelated sources, PCA and sPCA methods behave as described above. For correlated sources, sPCA still performs better than PCA, although, as natural, the sPCA strategy is much more robust in the case of uncorrelated sources. In this case, in fact, the orthogonality constraint in the time domain imposed by PCA and sPCA is correct but is violated in the case of correlated sources.

Conversely, the MOCA method behaves identically regardless of the correlation between the sources since the decomposition is based on purely spatial criteria. This method outperforms both PCA and sPCA for uncorrelated as well as for correlated sources. Actually, for uncorrelated sources, if one takes into account also the median values of the distributions together with the histograms, the sPCA median (M) is equal to $6 \cdot 10^{-4}$ whereas the median of the error distribution for the MOCA method is equal to $4 \cdot 10^{-4}$. This indicates that the higher rate of occurrence is obtained for lower error values for MOCA rather than for sPCA. This result is surprising as sPCA makes a dynamical assumption (in place of a stronger spatial one) that is exactly fulfilled in this case. Apparently, this is one of the rare cases where two errors have the tendency to compensate rather than to add up. In any event, both sPCA and MOCA are clearly far superior in comparison to PCA, the median value of which is equal to 0.1716 for uncorrelated sources.

In case of correlated sources, MOCA ($M=4 \cdot 10^{-4}$) clearly outperforms both PCA ($M=0.1160$) and sPCA ($M=0.0621$). For almost all of the simulated pairs of dipoles, in fact, the MOCA method strongly succeeds in the decomposition as indicated by an error value of less than 0.026. Only in the 2% of the 5000 tested pairs an error larger than 0.026 is found. These cases correspond to small values in the difference between the maximum and minimum in the MOCA cost function (21), which we defined as gap. The plot of the error of MOCA against the gap shows that, in fact, the worst errors are attained for the

smallest gap values. Note that this gap is attainable also in cases where we do not know the true solutions and hence we have indicator of the validity of the decomposition.

From this point on, we are mainly interested in further investigating the case of correlated source pairs. Supposing that the decomposition has been successfully accomplished, we now want to use the disentangled field patterns for localizing the position of the correlated source pairs in the brain. Since a dipole model is not always adequate to describe real sources in the brain apart from cases when the current source is highly localized (Williamson and Kaufman, 1981) and often no

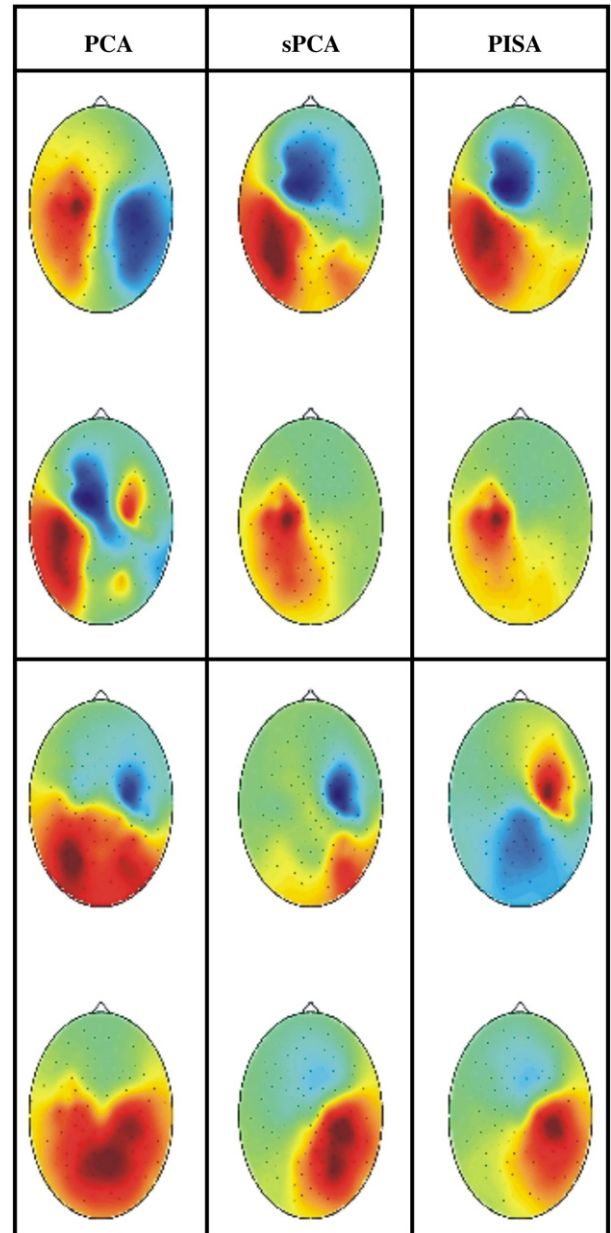


Fig. 5. Basis fields obtained from the imaginary part of the cross-spectra at 12 Hz (μ -rhythm) for MOCA rotated PCA decomposition, MOCA rotated sPCA decomposition, and basis fields ascribed to the μ -rhythm for the MOCA rotated PISA decomposition. The first two patterns on the top of each column correspond to the real and imaginary parts of the first complex eigenvector obtained by the decomposition of the imaginary part of the data cross-spectrum at 12 Hz accomplished by means of PCA and sPCA. Similarly, the 12-Hz component of the first basis field obtained by the PISA decomposition applied to the same data is shown. The other two patterns on the bottom of each column correspond to the real and imaginary parts of the second complex eigenvector of PCA and sPCA and to the 12-Hz component of the second basis field obtained by the PISA.

information regarding the spatial extent of the source distribution is known, one cannot generally rely on an ECD source model. In Fig. 4, we show, in fact, that when a multiple dipole-based method, such as the RAP-MUSIC scanning method (Mosher and Leahy, 1999), is used for the localization of a pair of correlated extended and distributed simulated sources, it fails in recovering the original source location (Liu, 2006).

The original extended and distributed sources are shown on the top right in Fig. 4. The first source is comprised by two active areas: one frontal area in the right hemisphere and one posterior area in the left hemisphere. The second source is the symmetric version of the first and is formed by one frontal area in the left hemisphere and one posterior area in the right hemisphere. The simulated field patterns corresponding to this source configuration are used for the source estimation with MOCA and with RAP-MUSIC. The comparison of the true sources with the ones obtained by MOCA and RAP-MUSIC clearly shows that only MOCA is able to recover the original source structure appropriately. The RAP-MUSIC solution provides two dipole locations, black dots, and a color-coded fit-quality distribution at the cortex points in which blue indicates low quality and red high quality fit. The results obtained with RAP-MUSIC show that this algorithm is only capable of partially localizing the centroid of some of the active areas comprising the original sources and is therefore not suitable for cases in which the source model cannot be a priori assumed to be point-like. We emphasize that this example is very artificial and merely serves to illustrate that our proposed methods also work in cases where the sources deviate substantially from dipoles.

Actual EEG data

In Figs. 5–7, we show the results obtained with the proposed MOCA method when applied to one example of actual EEG data.

In particular, Fig. 5 shows the application of the investigated methods to the μ rhythm of the actual EEG data. We recall that for PCA, sPCA, and PISA, the outcome is a two-dimensional subspace with ambiguous representation by two individual patterns. For all these three methods, we used MOCA for a unique representation.

We identify two compound systems by means of sPCA and PISA. Although the two methods take advantage of different properties in the data, they come to almost the same results in terms of system classification and source identification. In the sPCA case, the resulting basis fields are estimated for the 12-Hz component of the data. Conversely, in the PISA decomposition, the basis fields are extracted from the imaginary part of the cross spectrum in a large frequency range (0 to 45 Hz), and the spectral content of each basis field has to be classified a posteriori based on diagonal spectrum of each system. For these data, both of these methods distinguish between a left hemisphere system and a right hemisphere system with almost mirrored patterns. Furthermore, the estimated field patterns for each source within a system are very reasonable patterns corresponding to a central μ rhythm. The high similarity between the sPCA and PISA system classification and field patterns can be considered as an indicator of the robustness of the result. Conversely, the PCA results neither show any left to right symmetry between systems nor a clear meaning in each of the field patterns.

In Fig. 6, the fields of the μ rhythm derived from MOCA demixed PCA, sPCA, and PISA, respectively, are used as an input to RAP-MUSIC and MOCA in order to localize the sources within each system with results shown in Fig. 7. The RAP-MUSIC results for the 2D subspaces obtained by PCA, sPCA, and PISA, and the respective MOCA-weighted minimum norm results are shown as indicated. Reasonable results are provided by sPCA and PISA basis. Bilateral primary motor cortex (M1) and premotor cortex (PM) show up in the two systems.

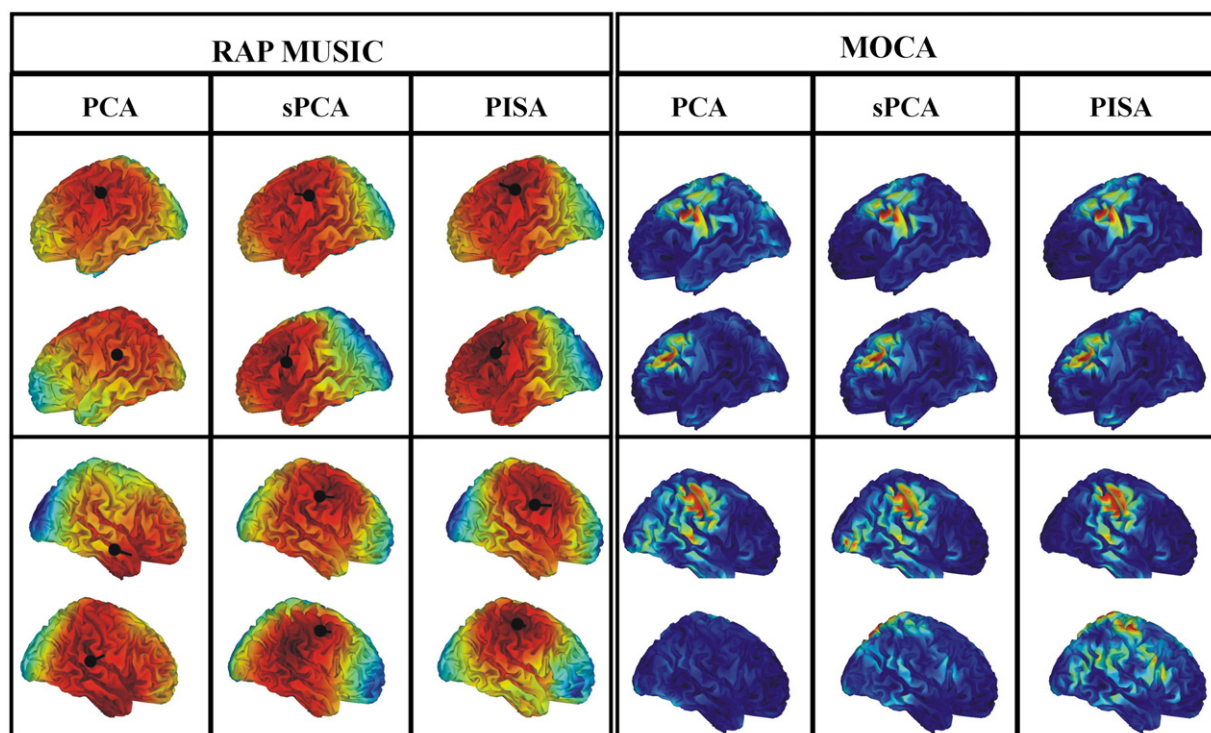


Fig. 6. RAP-MUSIC and MOCA-WMNE localization of the μ -rhythm patterns (12 Hz) shown in Fig. 5. The sources are correctly recovered by both methods.

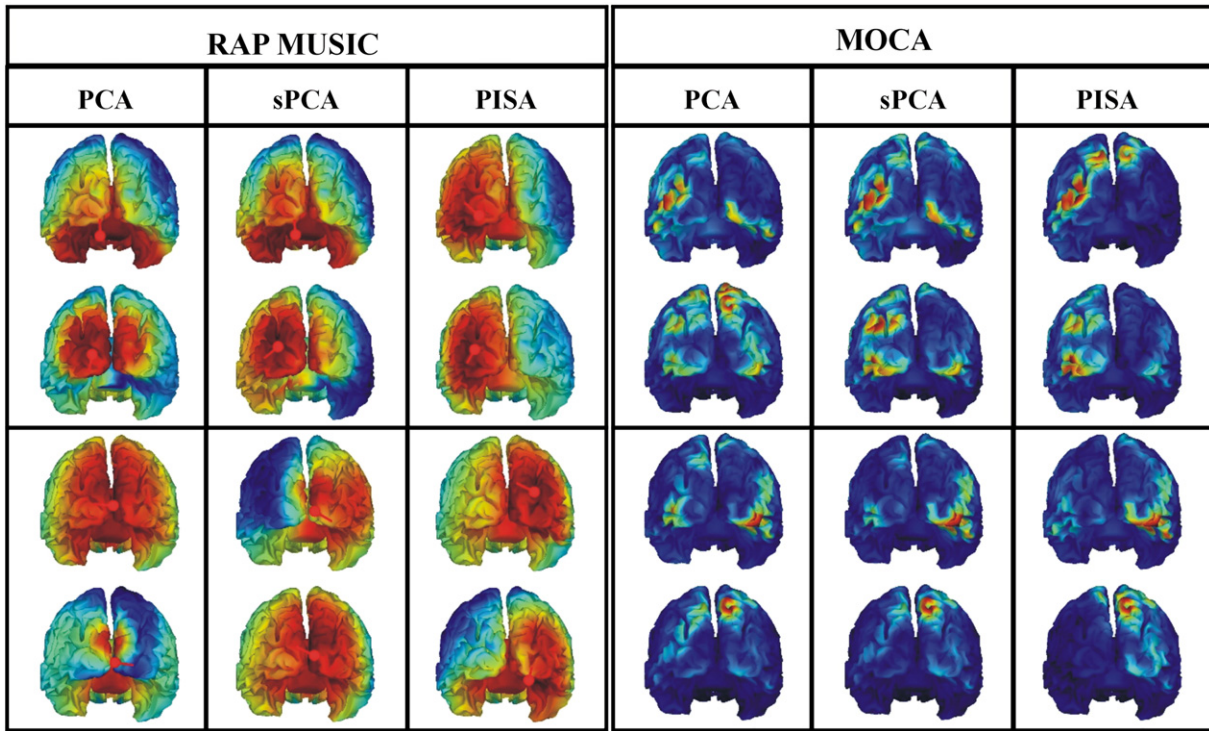


Fig. 7. RAP-MUSIC and MOCA-WMNE localization of the α -rhythm patterns (10 Hz) obtained by MOCA rotation of PCA, sPCA, and PISA, respectively. The sources are correctly recovered by MOCA-WMNE and wrongly recovered by RAP-MUSIC due to their extended and distributed nature.

Bilateral M1 is already known to be involved in generation of the spatiotemporal patterns of Rolandic μ rhythm in motor imagery (Pfurtscheller and Neuper, 1997). Moreover, interaction between left M1 and left PM in the 9- to 12-Hz frequency band has been also observed by Gross et al. (2001) using an ROI-based cortico-cortical coherence analysis.

The use of the RAP-MUSIC algorithm for inverse mapping provides, in this case, similar results, because of the focal nature of the involved area. Both the inverse algorithms are therefore able to reconstruct the sources roughly in the same location for the same basis fields in input. Note that the MOCA-localization of the PCA patterns shows a less reliable activation pattern with respect to the localization of sPCA and PISA patterns.

In Fig. 7, results for occipital α -rhythm are shown. Also in this case for sPCA and PISA, the sources localized by means of MOCA from the first basis field (first compound system) are mainly in the left hemisphere, whereas the sources localized from the second basis field (second compound system) are mainly located in the right hemisphere. This property does not hold for PCA basis fields, the localization of which results in a mixture of left and right sources.

Each system seems to be reasonably composed of occipital and parietal areas, consistently with the previously reported generators of spontaneous oscillatory activity in the α rhythm (Salmelin and Hari, 1994; Gross et al., 2001). Furthermore, some of the identified areas, such as the inferior parietal lobule and the intra parietal sulcus, are parts of the frontoparietal network obtained applying the graph theory to functional connectivity MRI data by Dosenbach et al. (2007).

From Fig. 7, it is also clear that these sources show up a distributed and extended nature rather than a well-localized one as for the motor μ rhythm. For this reason, when using RAP-MUSIC, it is hard to find convincing results.

Conclusions

This paper proposes a method for identifying compound systems in the brain and disentangling the contribution of the various sources within each system. In this work, we supposed that a compound system is composed of two dominating interacting sources, which have in general an extended and distributed nature. As a prerequisite, we developed the sPCA method for the decomposition of temporally uncorrelated or non-interacting sources, regarded to as the simplest possible system, which is more effective than classical PCA in separating the contribution of various brain sources to a measured field due to the assumption of spatial orthogonality of the sources rather than fields as assumed by classical PCA. We use this method in order to separate the contribution of various compound system each composed of one pair of interacting sources to the measured field. Computer simulations show that sPCA is able to disentangle the contribution of non-interacting sources to the global field whereas conventional PCA fails. Furthermore, results taking into account the influence of different types of noise show that sPCA does not degrade its performance also for a high noise level.

A second method, MOCA, is designed for the study of correlated source pairs and aims at disentangling the contribution of each source within a compound system by exploiting a purely spatial criterion. Nevertheless, since MOCA does not make any explicit assumption on the dynamical relationship between the source pairs, it performs well also for uncorrelated sources. The application of MOCA to each system identified by sPCA makes it possible to separate the two interacting sources within each system correctly. The MOCA approach provides also a weighted minimum norm localization of the decomposed source patterns, which is able to estimate focal as well as extended and distributed sources as opposite to the RAP-MUSIC scanning algorithm, which assumes dipolar sources.

The sPCA and MOCA methods were applied to the imaginary part of the cross-spectra of actual EEG data from a motor imagery protocol with the first method identifying compound systems, and the second separating sources within each of these systems. The sPCA system separation is in good agreement with the results provided by the PISA algorithm, which we applied for comparison, although the two methods have different theoretical basis. The MOCA decomposition applied to each system and the MOCA source localization shows that the primary motor and premotor areas interact at 12 Hz and occipital and parietal areas interact at 10 Hz in each hemisphere. When RAP-MUSIC is used to map the sources, meaningful source estimates are obtained only for the μ rhythm, the generators of which are typically focal.

We believe this approach can improve the understanding of brain interference phenomena by revealing networks formed by systems composed by sources interacting at a specific frequency or in a given frequency band. Therefore, we expect this method to be particularly effective in identifying interference among brain regions involved in the generation and keeping of human brain rhythms such as alpha rhythm for resting state activity or μ rhythm for somatomotor activity. We also believe that in all cases of pathologies in which an alteration of the power or frequency of such rhythms has been observed (e.g., Alzheimer disease), the method could contribute to the investigation of a possible alteration in the interaction mechanism as well.

Acknowledgments

This work was supported in part by Italian Ministry for University and Research, Grant PRIN 2005027850_001 and in part by the Bundesministerium fuer Bildung und Forschung (BCCNB-A4, 01GQ0415).

References

- Astolfi, L., Cincotti, F., Mattia, D., Marciani, M.G., Baccala, L.A., de Vico Fallani, F., Salinari, S., Ursino, M., Zavaglia, M., Ding, L., Edgar, C., Miller, G.A., He, B., Babiloni, F., 2007. Comparison of different cortical connectivity estimators for high-resolution EEG recordings. *Hum. Brain Mapp.* 28, 143–157.
- Baillet, S., Mosher, J., Leahy, R., 2001. Electromagnetic brain mapping. *IEEE Sig. Proc. Mag.* 18 (6), 14–30.
- Blankertz, B., Dornhenge, G., Schaefer, C., Krepki, R., Kohlmorgen, J., Mueller, K.-R., Kunzmann, V., Losch, F., Curio, G., 2003. Boosting bit rates and error detection for the classification of fast-paced motor commands based on single-trial EEG analysis. *IEEE Trans. Neural Syst. Rehabil. Eng.* 11 (2), 127–131.
- Brovelli, A., Battaglini, P.P., Naranjo, J.R., Budai, R., 2002. Medium-range oscillatory network and the 20-Hz sensorimotor induced potential. *NeuroImage* 16, 130–141.
- Crowley, C.W., Greenblatt, R.E., Khalil, I., 1989. Minimum norm estimation of current distributions in realistic geometries. In: Williamson, S.J., et al. (Ed.), *Advances in Biomagnetism*. Plenum, New York, pp. 603–606.
- David, O., Cosmelli, D., Friston, K.J., 2004. Evaluation of different measures of functional connectivity using a neural mass model. *NeuroImage* 21, 659–673.
- de Munck, J.C., van Dijk, B.W., Spekreijse, H., 1988. Mathematical dipoles are adequate to describe realistic generators of human brain activity. *IEEE Trans. Biomed. Eng.* 35 (11), 960–966.
- Dosenbach, N.U.F., Fair, A.D., Miezin, F.M., Cohen, A.L., Wenger, K.K., Dosenbach, R.A.T., Fox, M.D., Snyder, A.Z., Vincent, J.L., Raichle, M.E., Schlaggar, B.L., Petersen, S.E., 2007. Distinct brain networks for adaptive and stable task control in humans. *PNAS* 104 (26), 11073–11078.
- Evans, A.C., Kamber, M., Collins, D.L., MacDonald, D., 1994. An MRI-based probabilistic atlas of neuroanatomy. In: Shorvon, S., et al. (Ed.), *Magnetic Resonance Scanning and Epilepsy*. Plenum, New York, pp. 263–274.
- Gevins, A., 1989. Dynamic functional topography of cognitive task. *Brain Topogr.* 2, 37–56.
- Gross, J., Kujala, J., Hämäläinen, M.S., Timmermann, L., Schnitzler, A., Salmenin, R., 2001. Dynamic imaging of coherent sources: studying neural interactions in the human brain. *PNAS* 98 (2), 694–699.
- Hämäläinen, M.S., 1993. Magnetoencephalography—theory, instrumentation, and applications to non invasive studies of working human brain. *Rev. Mod. Phys.* 65, 413–497.
- Hämäläinen, M.S., Ilmoniemi, R.J., 1984. Interpreting Measured Magnetic Fields of the Brain: Estimates of Current Distributions. Helsinki Univ. of Technol., Rep. TKK-F-A559.
- Hämäläinen, M.S., Ilmoniemi, R.J., 1994. Interpreting magnetic fields of the brain: minimum norm estimates. *Med. Biol. Eng. Comput.* 32, 35–42.
- Hyvarinen, A., Karhunen, J., Oja, E., 2001. *Independent Component Analysis*. Wiley, New York.
- Jolliffe, I.T., 1986. *Principal Component Analysis*. Springer-Verlag, New York.
- Horwitz, B., 2003. The elusive concept of brain connectivity. *NeuroImage* 19, 466–470.
- Kendall, M., 1975. *Multivariate Analysis*. Charles Griffin & Co, London.
- Lee, L., Harrison, L.M., Mechelli, A., 2003. The functional brain connectivity workshop: report and commentary. *NeuroImage* 19, 457–465.
- Liu, H., 2006. Efficient localization of synchronous EEG source activities using a modified RAP-MUSIC algorithm. *IEEE Trans. Biomed. Eng.* 53 (4), 652–661.
- Marzetti, L., Nolte, G., Perrucci, G., Romani, G.L., Del Gratta, C., 2007. The use of standardized infinity reference in EEG coherency studies. *NeuroImage* 36, 48–63.
- Mosher, J., Leahy, R., 1999. Source localization using recursively applied and projected (RAP) music. *IEEE Trans. Signal. Proc.* 47 (2), 332–340.
- Nolte, G., Dassios, G., 2005. Analytic expansion of the EEG lead field for realistic volume conductors. *Phys. Med. Biol.* 50 (16), 3807–3823.
- Nolte, G., Bai, U., Weather, L., Mari, Z., Vorbach, S., Hallet, M., 2004. Identifying true brain interaction from EEG data using the imaginary part of coherency. *Clin. Neurophysiol.* 115, 2294–2307.
- Nolte, G., Meinecke, F.C., Ziehe, A., Mueller, K.-R., 2006. Identifying interactions in mixed and noisy complex system. *Phys. Rev. E* 73, 051913.
- Nunez, P.L., Srinivasan, R., Westdorp, A.F., Wijesinghe, R.S., Tucker, D.M., Silberstein, R.B., Cadusch, P.J., 1997. EEG coherency I: statistics, reference electrode, volume conduction, Laplacians, cortical imaging, and interpretation at multiple scales. *Electroencephalogr. Clin. Neurophysiol.* 103 (5), 499–515.
- Nunez, P.L., Silberstein, R.B., Shi, Z., Carpenter, M.R., Srinivasan, R., Tucker, D.M., Doran, S.M., Cadusch, P.J., Wijesinghe, R.S., 1999. EEG coherency II: experimental comparison of multiple measures. *Clin. Neurophysiol.* 110 (3), 469–486.
- Pascal-Marqui, R.D., 1999. Review of methods for solving the EEG inverse problem. *Int. J. Bioelectromag.* 1 (1), 75–86.
- Pascal-Marqui, R.D., Michel, C.M., Lehmann, D., 1999. Low resolution electromagnetic tomography: a new method for localizing electrical activity in the brain. *Int. J. Psychophysiol.* 18 (1), 49–65.
- Pfurtscheller, G., Neuper, C., 1997. Motor imagery activates primary sensorimotor area in humans. *Neurosci. Lett.* 239, 65–68.
- Pfurtscheller, G., Lopes da Silva, F.H., 1999. Event-related EEG/MEG synchronization and desynchronization: basic principles. *Clin. Neurophysiol.* 110 (11), 1842–1857.
- Salmelin, R., Hari, R., 1994. Characterization of spontaneous MEG rhythms in healthy adults. *Electroencephalogr. Clin. Neurophysiol.* 91 (4), 237–248.
- Sekihara, K., Scholz, B., 1996. Generalized Wiener estimation of three-dimensional current distribution from biomagnetic measurements. *IEEE Trans. Biomed. Eng.* 43 (3), 281–291.
- Taniguchi, M., Kato, A., Fujita, N., Hirata, M., Tanaka, H., Kihara, T., Ninomiya, H., Hirabuki, N., Nakamura, H., Robinson, S.E., Cheyne, D., Yoshimine, T., 2000. Movement-related desynchronization of the cerebral cortex studied with spatially filtered magnetoencephalography. *NeuroImage* 12 (3), 298–306.
- Wang, J.Z., Williamson, S.J., Kaufman, L., 1992. Magnetic source images of determined by a lead-field analysis: the unique minimum norm least squares estimation. *IEEE Trans. Biomed. Eng.* 39, 565–575.
- Williamson, S.J., Kaufman, L., 1981. Biomagnetism. *J. Magn. Magn. Mater.* 22, 129–201.